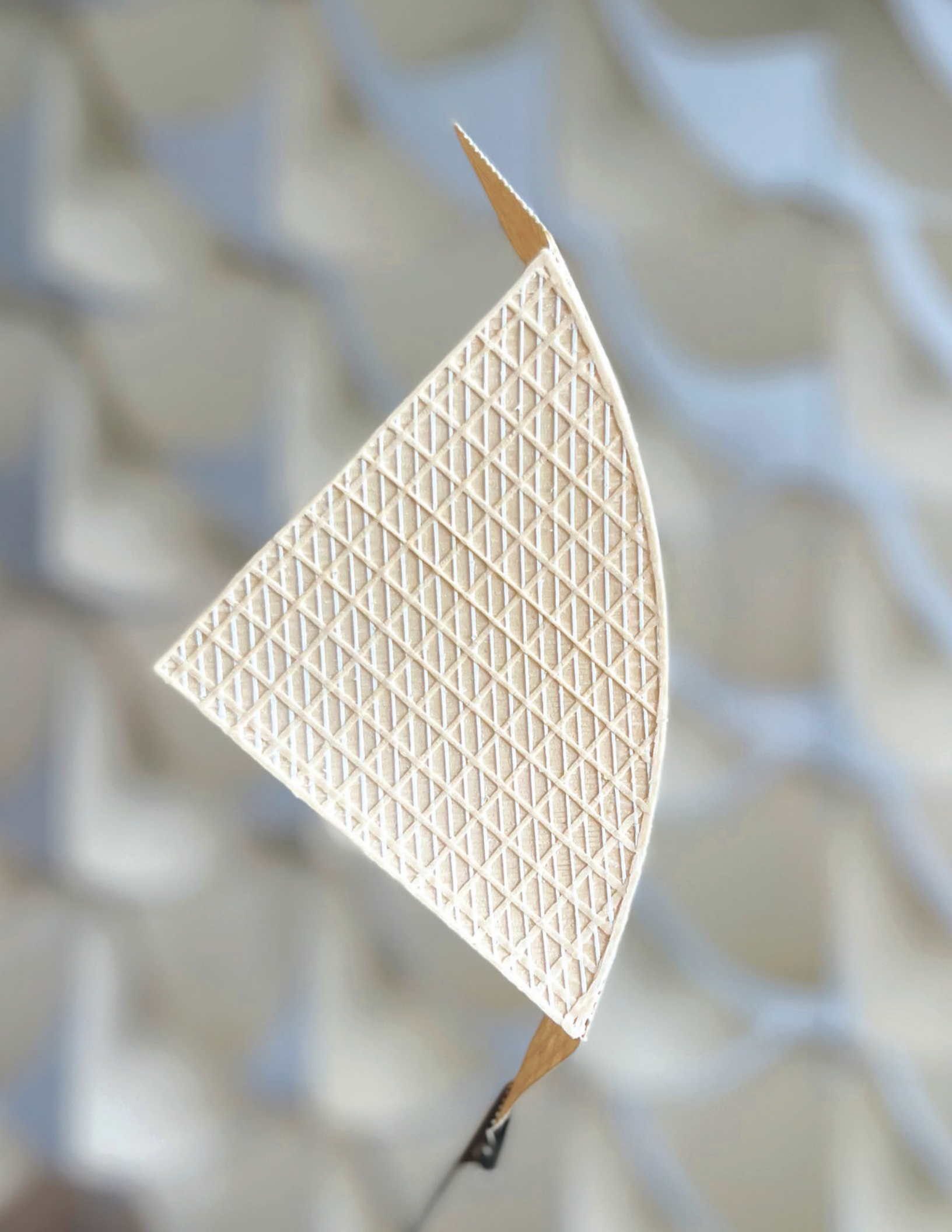

3D PRINTING AND ADDITIVE MANUFACTURING
Volume 10, Number 1, 2023
Mary Ann Liebert, Inc.
DOI: 10.1089/3dp.2022.0061

ORIGINAL ARTICLE

Codesign of Biobased Cellulose-Filled Filaments and Mesostructures for 4D Printing Humidity Responsive Smart Structures

Yasaman Tahouni,[1,2] Tiffany Cheng,[1,2] Silvia Lajewski,[3] Johannes Benz,[3] Christian Bonten,[3] Dylan Wood,[1,2] and Achim Menges[1,2]

Abstract

Hygromorphic smart structures are advantageous as passively actuated systems for generating movement, with applications ranging from weather-responsive architectural building skins to adaptive wearables and microrobotics. Four-dimensional (4D) printing is a valuable method for multiscale fabrication and physical programming of such structures. However, material limitations in terms of printability, responsiveness, and mechanical properties are major bottlenecks in achieving reliable and repeatable humidity-responsive actuation. We propose a codesign method for 4D printing hygromorphic structures through fused filament fabrication, incorporating parallel development of (1) biobased cellulose-filled filaments with varying stiffness and hygroresponsiveness, and (2) designed mesoscale structuring in printed elements. We first describe the design of a pallet of filaments produced by compounding cellulose powder in mass ratios of 0–30% within two matrix polymers with high and low stiffness. We then present the design, fabrication, and testing of a series of 4D-printed prototypes tuned to change shape, that is, open and close, in response to relative humidity (RH). The structures can fully transform in conditions of 35–90% RH, which corresponds to naturally occurring shifts in RH in daily and seasonal weather cycles. Furthermore, their motion is fast (within the range of minutes), fully reversible, and repeatable in numerous cycles. These results open new opportunities for the utilization of 4D printing and natural resources for the development of functional humidity-responsive smart structures.

Keywords: fused filament fabrication, biobased polymers, hygromorphs, material programming, adaptive architecture

Introduction

The building and construction sector is responsible for 36% of global energy consumption and 39% of energy- and process-related carbon dioxide (CO_2) emissions.[1] Thus, the reduction of operational energy related to heating, ventilation, and air conditioning in buildings represents a major growing ecological challenge. This makes adaptive shading elements and weather-responsive building envelopes increasingly important. Hygroresponsive smart structures offer

[1]Institute for Computational Design and Construction (ICD), University of Stuttgart, Stuttgart, Germany.
[2]Cluster of Excellence Integrative Computational Design and Construction for Architecture (IntCDC), University of Stuttgart, Stuttgart, Germany.
[3]Institut für Kunststofftechnik (IKT), University of Stuttgart, Stuttgart, Germany.

Opposite page: A 4D printed humidity-responsive curved folded mechanism and its multi-layered mesostructure composed of a palette of biobased filament materials. *Image Credit:* ICD University of Stuttgart.

novel ways to address this challenge in building skins.[2–4] These structures are able to change their shape autonomously in response to changes in the environment's relative humidity (RH),[5] which is a function of both absolute humidity and temperature. By integrating functions of sensing, computation, and actuation within their material composition and structuring, they can execute their movement without requiring electromechanical sensors and actuators or external power supply.

This movement can be utilized to create building envelopes that open and close autonomously in response to shifts in weather conditions,[3,4,6–8] among other applications such as textile and wearables that adapt to the human body[9–12] and hygroactuated microrobotics.[13–15]

Four-dimensional (4D) printing, which refers to the three-dimensional (3D) printing of structures that can change their shape over time in response to external stimuli,[16] is a suitable method for the development of hygromorphic smart structures. The core of such process involves using 3D-printable base materials that are responsive to external stimuli, and the design of mechanisms and material structuring in 3D-printed elements, which dictates their preprogrammed shape change.[17–19] Recent advances in their design and manufacturing methods have showcased 4D-printed hygromorphic structures with tunable characteristics at meso- to macroscales[20,21] and programmable shape change.[22,23] However, the development of materials suitable for stimuli response in targeted actuation ranges, with desirable mechanical properties, and compatible with 3D printing processes remains a challenge.

The current state of the art has explored a variety of material systems including hydrogel composites,[20,24–26] spore-based materials,[9,27] and natural fiber biocomposites.[21,28–31] Among these, natural fiber biocomposites are advantageous due to their use of natural material resources, their enhanced mechanical properties,[28,32] and their processability with the highly accessible and scalable fused filament fabrication (FFF) technique.[33] However, their use in 4D printing has been largely limited to off-the-shelf ''wood''-filled filaments.[33,34] This has resulted in major shortcomings in the responsiveness and functionality of the 4D-printed structures, including weak reversibility and repeatability of motion in cyclic actuation,[21,28] lack of responsiveness to environmental RH rather than water immersion,[21,35] short life spans due to delamination of incompatible material layers,[22] and lack of control over the mechanical properties of the materials. Furthermore, material engineering and design and manufacturing techniques are often studied independently, failing to reach comprehensive solutions for specific use cases.

We hypothesize that an integrative approach that combines targeted material engineering with digital design and manufacturing can overcome the aforementioned limitations and facilitate practical application of 4D printing.

This article presents the codesign of filament materials for FFF 3D printing and the design of printed structures in different length scales to achieve humidity responsive shape change (Fig. 1). The term codesign refers to the integrative, interdisciplinary, and feedback-driven development of computational design and engineering methods, digital fabrication processes, as well as the development of related material and building systems.[36] We present the development of a pallet of cellulose-filled filaments with varying stiffness and hygroscopic filler content, which are by design targeted for

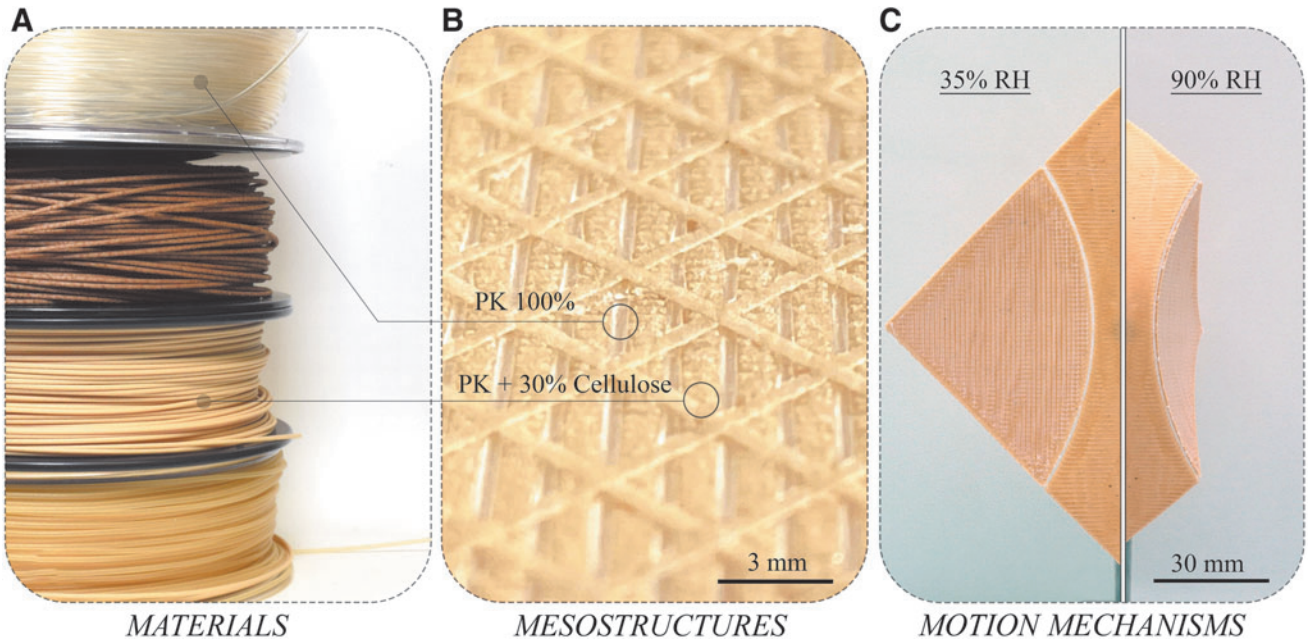

FIG. 1. Codesign for 4D printing. **(A)** Development of a palette of custom hygroscopic printing filaments composed of biobased matrix polymers and cellulose powder. **(B)** Detailed view of the 3D-printed, multimaterial mesostructures with designed anisotropy and porosity. **(C)** Humidity-responsive smart structure based on curved folding mechanism with actuated surfaces and flexible hinges in near-flat configuration equalized in 35% RH (*left*), and folded configuration in 90% RH (*right*; in 20°C). 3D, three dimensional; 4D, four dimensional; RH, relative humidity.

maximum responsiveness and shape change (Fig. 1A). By using complementary hygroscopic and passive materials in functional bilayer structures, and by arranging the anisotropic material structuring in each layer (Fig. 1B), hygromorphic structures are produced.

We present a series of 4D-printed hygromorphic structures that change their shape in response to changes in RH (Fig. 1C). Through comprehensive testing of the prototypes in a climate-controlled environment, we showcase their reliable, cyclic, and amplified motion. These results demonstrate the potential of the developed 4D-printed smart structures for practical applications, such as in weather-responsive building envelopes.

Materials and Methods

Production of filament materials

Biocomposite filament materials were produced by compounding native cellulose powder (sourced from JELUCEL HM30; JELU-WERK, Rosenberg, Germany) and two partially biobased thermoplastic matrix polymers, namely, thermoplastic polyurethane (TPU; Pearlthane ECO D12T90E; Lubrizol) and polyketone (PK; AKROTEK PK-VM natural; AKRO-PLASTIC, Niederzissen, Germany). The filament production followed a three-step process (Supplementary Fig. S1), First, all materials were dried under vacuum, with drying time varying according to the respective initial moisture content. Next, granules were produced by compounding the cellulose powder and matrix polymers using a ZSK26 twin-screw extruder from Coperion (Stuttgart, Germany).

Finally, the compounds were extruded into filaments with a constant diameter of 1.75 mm (±0.1 mm) using a laboratory extrusion line from Collin (Maitenbeth, Germany). To ensure the dimensional accuracy of the produced filaments, they were continuously measured with a Zumbach ODAC 15XY-J Laser Micrometer and WIREMASTER from Keyence (Neu-Isenburg, Germany). In addition to the customized filament, a generic PLA filament (Geeetech; HK Getech Co.) was used in printing standardized samples.

Fused filament fabrication

A standard dual-extruder FFF 3D printer (FELIX TEC 4; FELIX printers, IJsselstein, The Netherlands) was used to print all the samples and prototypes. The 3D printer was equipped with one 0.7 mm hardened steel nozzle (used for extruding the cellulose-filled filaments) and one 0.4 mm brass nozzle (used for extruding the pure polymer filaments). The 3D printing G-codes were generated using a custom-built software tool built in the Grasshopper visual programming environment (Grasshopper 3D) and Rhino CAD software (RhinoCeros 3D; McNeel & Associates), which allowed a seamless transition between the design and fabrication steps.[37] All 3D printing toolpaths were parametrically designed. The toolpaths were first generated as anisotropic two-dimensional (2D) hatches with defining parameters of the orientation (in the *X-Y* plane) and spacing (S_a and S_r) (Fig. 2B).

After generating the 2D paths, they were moved in the *Z* direction, with defining parameters of layer height (*H*) and the number of layers (N_a and N_r) (Fig. 2B). After generating all toolpaths, each set of toolpaths was assigned with specific material. The 3D printing parameters, including nozzle temperature, bed temperature, printing speed, and material flow, were then automatically assigned according to the optimal values found by an experiment (Table 1). In the bifold prototypes, three materials were used for printing the prototypes. In this study, the G-code was generated in two separate files, and the filaments were changed manually between running the two G-codes on the 3D printer.

Mesostructure setup

A functional bilayer scheme was used as the basic construct for producing hygromorphic structures (Fig. 2A). The bilayer constructs are composed of a hygroscopic active layer, printed with cellulose-filled filaments in multiple printed layers, and a moisture-stable restrictive layer, printed with pure polymers. In the basic setup, the active layer is printed in two layers with a layer height of 0.26 mm, a spacing within the range of 0.85–1.0 mm, and transversal

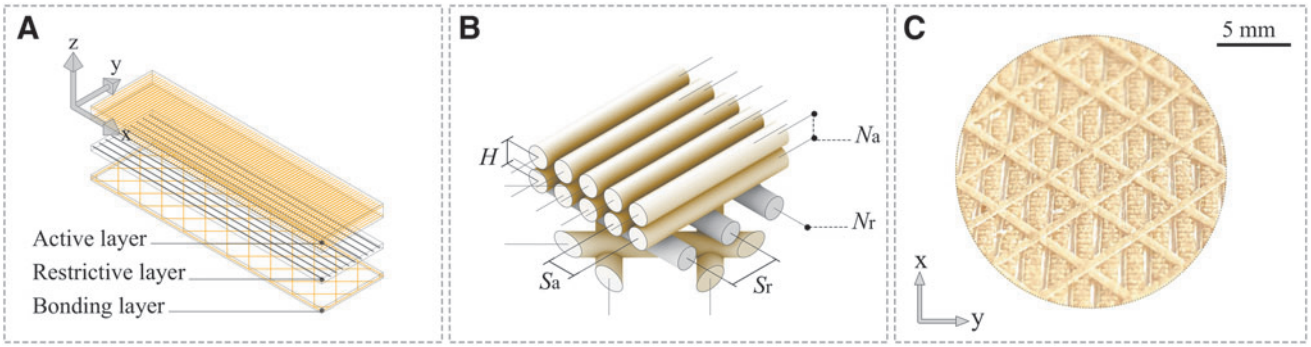

FIG. 2. Mesostructure design and correlated toolpath design parameters. **(A)** Mesostructure and toolpath arrangement of a basic bilayer construct consisting of active, restrictive, and bonding layers. **(B)** Toolpath design parameters: S_a and S_r indicate the spacing between adjacent toolpaths in the active and the restrictive layers, N_a and N_r indicate the number of layers in the active and the restrictive layers, and *H* indicates the layer height. **(C)** Resulting 3D-printed mesostructure (the photograph shows the underside of the printed structure, with the bonding and the restrictive layers visible on top).

Table 1. Optimal 3D Printing Parameters

Matrix polymer	*Filler content (%)*	*Abbreviation*	*Nozzle size*	*Nozzle temperature (°C)*	*Bed temperature (°C)*	*Printing speed (mm/min)*	*Material flow (%)*
TPU	0	TPU100%	0.4	210	55	800–1200	150
TPU	10	TPU90%	0.7	210	55	800–1200	150
TPU	30	TPU70%	0.7	210	55	800–1200	150
PK	0	PK100%	0.4	230	75	800–1200	100
PK	10	PK90%	0.7	230	75	800–1200	100
PK	30	PK70%	0.7	230	75	800–1200	120

The values are experimentally found for each filament, characterized by the matrix polymer and the filler content.
PK, polyketone; TPU, thermoplastic polyurethane.

orientation in the *X-Y* plane. The restrictive layer is printed in one layer with a layer height of 0.20 mm, a spacing of 2 mm, and longitudinal orientation in the *X-Y* plane.

In addition to the active and the restrictive layer, an optional ''bonding layer'' can be added to the functional bilayer scheme (Fig. 2A). This layer is printed using the active layer material, and it partially holds the restrictive layer between two compatible material layers that adhere well together, thus helps preventing global layer delamination.[35] The bonding layer is always printed as a bidirectional hatch with +45° and −45° angles in the *X-Y* plane and high porosity (spacing >4 mm), which helps minimize its stiffness and its effect on the shape-change of the functional bilayer.

Beyond the basic setup, the FFF toolpath design parameters can be adjusted to tune the mesostructural anisotropy and porosity, thus physically programming the shape-change in bilayer constructs. By orienting the printing paths of the active layer perpendicularly to the desired bending orientation, longitudinal, transversal, or twisting shape-change can be achieved[12,21] (Supplementary Fig. S2B). The convex or concave bending direction of bilayers can be changed by switching the order of printing of the active and restrictive layers (Supplementary Fig. S2B).

Lastly, the bending curvature can be controlled through multiple strategies, including variations in the thickness of layers (controlled by the number of printed layers), and variations in the filling ratio of the restrictive layer (controlled by the spacing parameter).[23,38] The maximum curvature in printed bilayers can be reached with the composition of one restrictive layer and two or three active layers, assuming the same layer height in all layers (Supplementary Fig. S2C). While keeping the number of layers constant, the curvature of bilayers can be reduced by decreasing the spacing parameter in the restrictive layer[38] (Supplementary Fig. S2D).

Actuation testing and documentation

To examine the responsiveness of the printed structures to ambient RH, an active microclimate generator (MiniOne; Preservatech, Bydgoszcz, Poland) attached to a glass container with dimensions of $50 \times 50 \times 50$ cm was used. The temperature in the chamber was kept consistent at 19–22°C, and the RH was set at values in the range of 30–95%. For stepwise actuation experiments, as shown in Figure 3, the RH was increased incrementally within intervals of 10%. At each step, the RH was kept constant for a period of 3 h, which allowed the prototype to equalize with the environment and reach its final curvature.

For short-term and long-term cyclic actuation, the RH was set to switch between the high and low values within the intervals of 3 h. To measure the rate of shape-change during absorption and desorption cycles, the aperture was immediately moved between the humidity-controlled chamber with preset 90% RH, and the room environment with controlled 35% RH. To examine the shape-change of printed samples due to water immersion, the samples initially equalized at 30% RH were placed in a water tank at room temperature (25°C) for 12 h. To characterize the mechanical properties of materials, tensile tests based on DIN EN ISO 527-1 were performed on three printed tensile bars (per material) using the 1476 universal testing machine from Zwick GmbH & Co. KG (Ulm, Germany).

The shape-change of the samples was documented by time-lapse photography (Sony Alpha 6100) taken within intervals of 60 s. In bilayer strip samples, the curvature measurement was performed on the time-lapse images, taken from the side-view, using ImageJ software.[39] For each image, three points (two ends and the middle) were chosen on a sample to define a triangle, and the radius of the circumcircle was calculated using a script[40] (Supplementary Fig. S3). To calculate the fold angle in the bifold module from the side-view images, the distance between the tip and the midpoint of the curved crease was measured (Supplementary Fig. S3). The cosine of the fold angle was calculated by dividing this value over the distance between the tip and the midpoint of the curved crease in the flat prototype. In long-term cyclic experiments, the area measurements were performed through image processing using MATLAB.

Results

Cellulose-filled filament materials for 4D printing

A pallet of stiff and flexible, pure and cellulose-filled filaments was produced by compounding different ratios of cellulose powder with thermoplastic matrix polymers (Fig. 3A). Cellulose powder was chosen as the hygroscopic filler due to its high hygroscopic property, its abundance as a natural material, and its favorable mechanical properties for manufacturing purposes.[34] The matrix polymers were

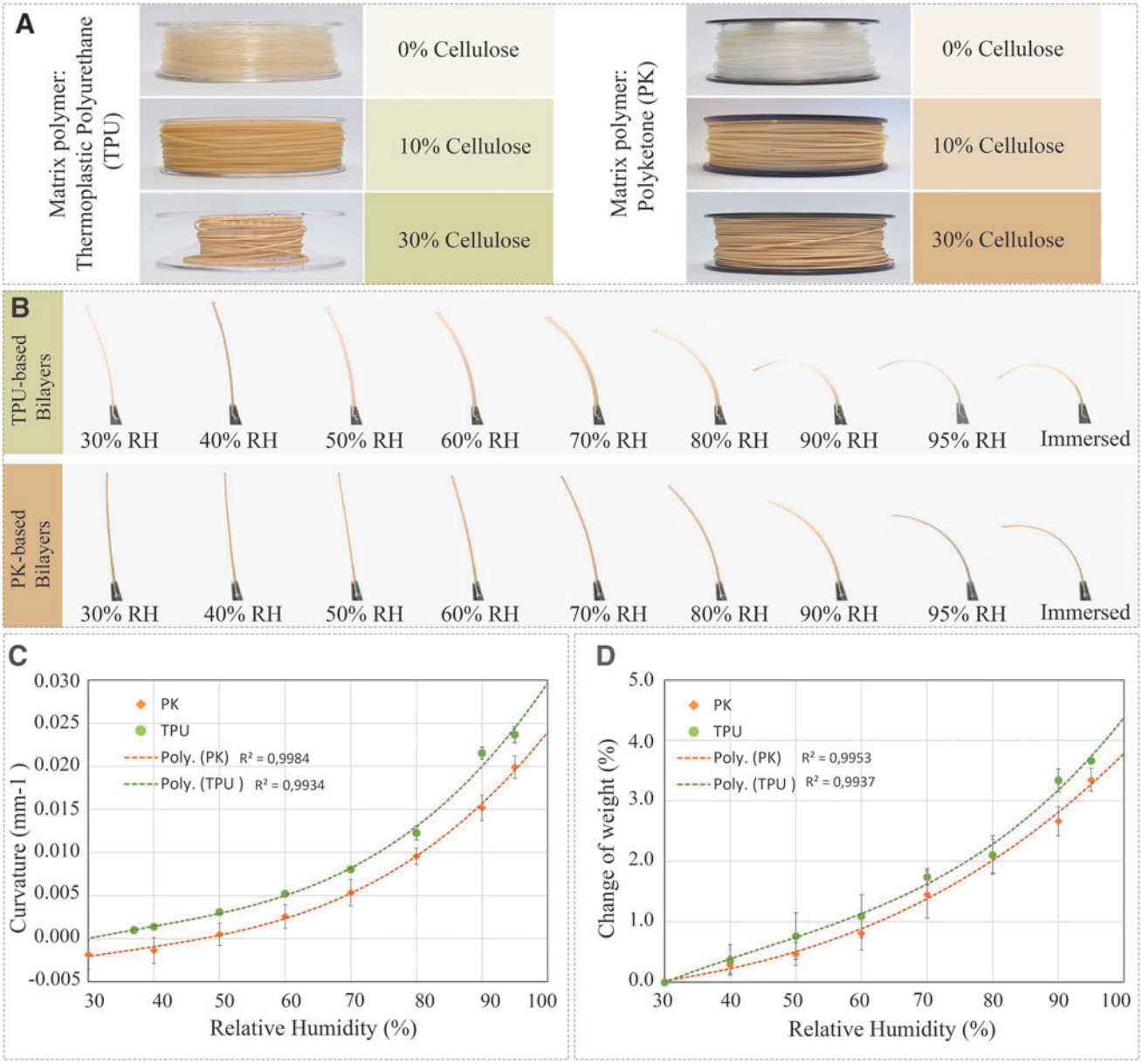

FIG. 3. Hygroscopic biocomposite filaments and humidity-responsive 3D-printed bilayers. **(A)** The palette of six filaments based on two matrix polymers of PK and TPU with 0%, 10%, and 30% cellulose content (mass ratio). **(B)** 3D-printed bilayer constructs and their bending after equalization in stepwise RH levels and water immersion. **(C)** Change of curvature in 3D-printed bilayers in stepwise RH levels ($n = 5$ per set/material). **(D)** Change of weight of 3D-printed bilayers in stepwise RH levels ($n = 5$ per set/material). PK, polyketone; TPU, thermoplastic polyurethane.

selected for their FFF printability and mechanical properties. Several criteria were established for engineering these materials. First, low brittleness was desired to achieve high morphing capability in the produced biocomposites.[41,42] Second, both flexibility and stiffness were desired to provide freedom for designing and fabricating a range of compliant motion mechanisms.

Based on these criteria, biobased TPU with a tensile strength of 37 MPa and an ultimate elongation of 470% was chosen to create flexible filaments, and biobased PK with a Young's modulus of 1500 MPa and an ultimate elongation of 200% was chosen to produce relatively stiff filaments. The choice of the two matrix polymers was also informed by preliminary studies,[42] which showed their high hygroscopic shape-change compared with the biocomposites based on stiff and brittle matrix polymers such as PLA and PHBV. The cellulose powder was compounded with the two matrix polymers with mass ratios of 0/100, 10/90, and 30/70, resulting in a pallet of six filaments (Fig. 3A).

To evaluate the printability of the produced filaments, a series of experiments were performed, in which the 3D printing parameters were systematically varied, and the optimum parameter values were found (Table 1). All filaments are printable on a generic FFF 3D printer with typical nozzle temperatures within the range of 210–

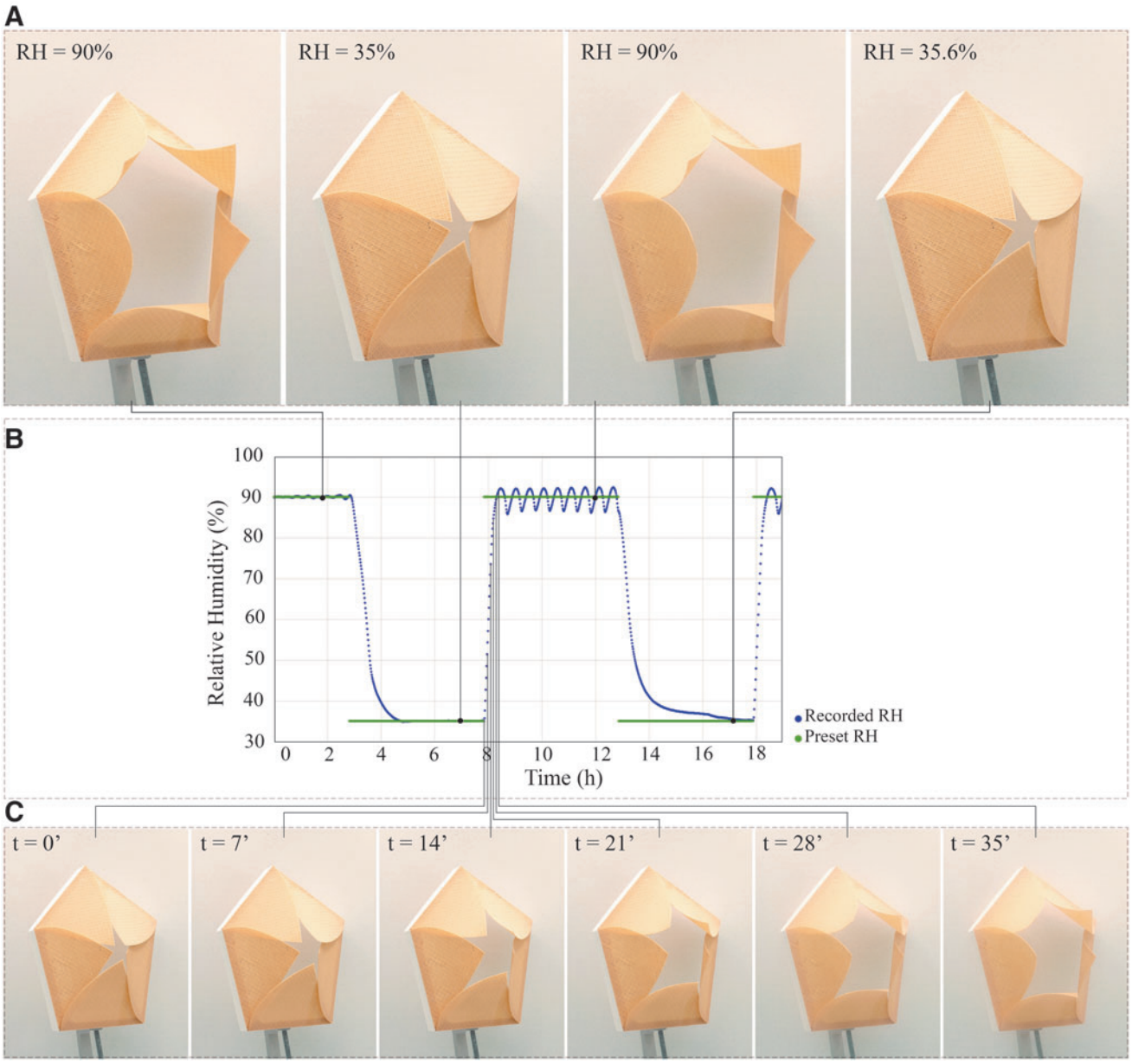

FIG. 4. Cyclic, humidity-responsive shape-change of the aperture prototype. **(A)** In 90% RH, the flaps bend outward and the aperture opens, while switching to 35% RH causes the aperture to close. **(B)** Indication of the RH level in the testing chamber, showcasing two full cycles between 90% and 35% RH. **(C)** Transition of the aperture between closed to open state within the time frame of 35 min, following the change of RH level in the testing chamber (Supplementary Movie S1).

230°C and bed temperatures within the range of 55–75°C. When printing with PK-based filaments at 55°C, warping often occurred after printing three layers, but increasing the bed temperature to 75°C allowed smooth printing for up to eight layers. Occasional clogging occurred when printing filaments with 30% cellulose content with the default 0.4 mm nozzle, which was solved by switching to a 0.7 mm nozzle.

To achieve a consistent extrusion, the material flow percentage was increased when printing the flexible and cellulose-filled filaments. The TPU-based filaments showed the best printability and resultant surface quality with 150% or a higher material flow rate, and the PK70% filament showed the best printability with 120% or a higher flow rate. A lower flow rate can create occasional under extrusion caused by clogging, which results in unintentional gaps on the printed surface. To compensate for the over extrusion caused by the increased flow rate, the spacing parameter in the active layer was adjusted accordingly to 1 mm (when printing with TPU70%) and 0.85 mm (when printing with PK70%).

To characterize the mechanical properties of the produced materials, tensile tests were performed on 3D-printed tensile test bars (Supplementary Fig. S4). In TPU-based materials, the Young's modulus increases from 34.7 MPa (in TPU100% filaments) to 68.07 MPa (in TPU70% +30% cellulose filaments). In parallel, the elongation at break

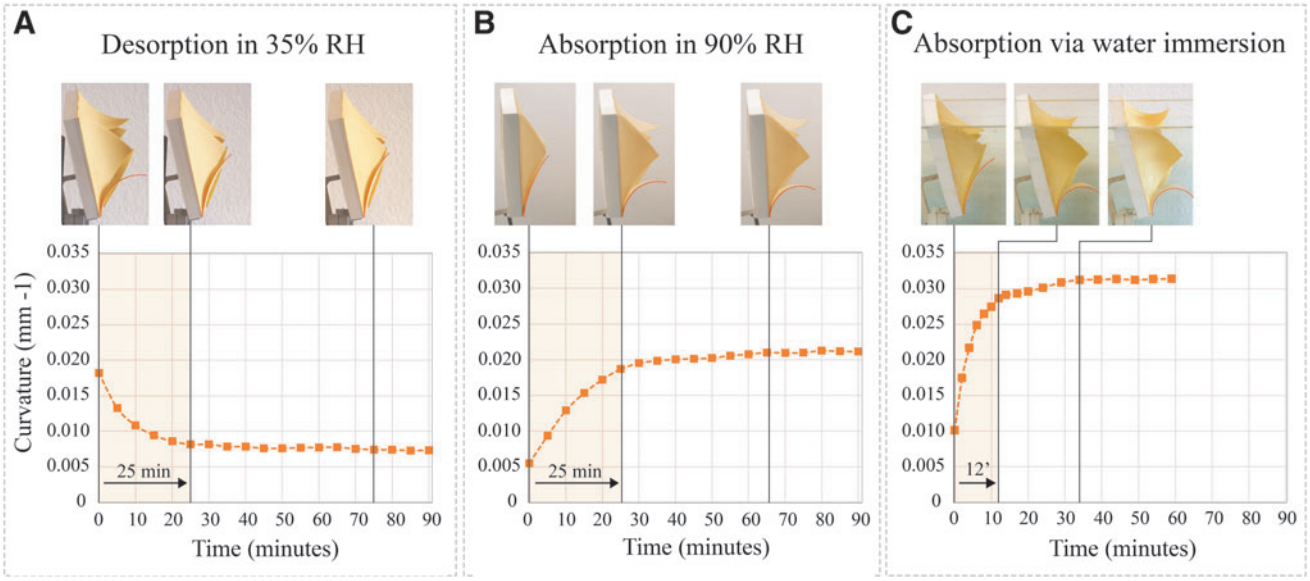

FIG. 5. Evolution of curvature as a function of time in the aperture prototype. **(A)** During desorption in 35% RH (from initial equalization in 90% RH). **(B)** During absorption in 90% RH (from initial equalization in 35% RH). **(C)** During absorption through water immersion (from initial equalization in 35% RH). The curvature is measured on the lower flap, indicated with *red* markings on the photographs. The three *points* marked on each graph represent the initial state, the time at which the structure reaches more than 90% of its final shape-change, and the final equalized state.

decreases from 120% to 54.6%. These results are in line with the expectations that the fibrous cellulose filler increases the stiffness and decreases the flexibility of the material. The PK-based filaments, on the contrary, showcase a much higher stiffness and lower elasticity range. In the PK70% test bars, a Young's modulus of 1345 MPa and an elongation at break of 2.15% were measured. Unfortunately, due to the high warping of PK100% filament, tensile test bars could not be properly printed, and thus, there are no comparative values for comparing the filled and unfilled PK-based materials.

A final comparison can be made between the flexible TPU70% and stiffer PK70% filaments. Comparing the two, a ratio of 1976% in Young's modulus and a ratio of 0.04% in elongation at break are observed, indicating the prominent effect of matrix polymer on the stiffness of the cellulose-filled filaments.

Evaluation of responsiveness in mesostructured functional bilayers

Using the pallet of biocomposite filaments, a series of standardized functional bilayer constructs were printed and tested. The functional bilayers are composed of active, restrictive, and bonding layers with a mesostructural arrangement, as illustrated in Figure 2A. In all samples, the toolpath design parameters have been set according to the basic setup described in the Methods section. To allow benchmarking of different biocomposite active materials, the restrictive layers were printed using a generic PLA filament. The samples were then examined for their shape-change in response to environmental RH changes and water immersion (Fig. 3), following the testing procedure explained in the Methods section.

Among all samples, bilayers in which the active layer was produced with filaments with 30% cellulose content exhibited the largest transformation upon water immersion. The bilayers produced with TPU70% and PK70% reached an average curvature of 0.026 and 0.023 mm^{-1}, respectively, in the wet state. In contrast, samples produced with filaments containing 10% cellulose reached a significantly lower curvature, with samples produced with TPU90% and PK90% filaments reaching an average curvature of 0.008 and 0.002 mm^{-1}, respectively. This is due to the effect of the cellulose content on the hygroscopic swelling capability of materials, which results in a higher curvature upon moisture absorption in samples with a higher cellulose content.

To evaluate the responsiveness of bilayers to ambient RH, samples produced with TPU70% and PK70% filaments were further examined in the humidity-controlled chamber (Fig. 3B). The change of weight and curvature of samples ($n = 5$ per material) corresponding to 10% change in the environment's RH is shown in Figure 3C and D. The results indicate a substantial increase in weight and curvature of the samples due to moisture absorption in response to increases in the environment's RH. On average, samples produced with the PK-based filament reached a final curvature of 0.020 mm^{-1} in 95% RH, and TPU-based samples reached 0.024 mm^{-1} curvature in 95% RH. A comparison between the maximum curvature (reached upon water immersion) and the curvature at 95% RH shows that both samples can reach more than 90% of their maximum curvature in response to humidity, which indicates their high humidity responsiveness.

In parallel, a comparison can be made between the two matrix polymers: in general, the bilayer samples printed with the flexible TPU-based filament showcase a larger shape-change compared with the PK-based samples in all RH

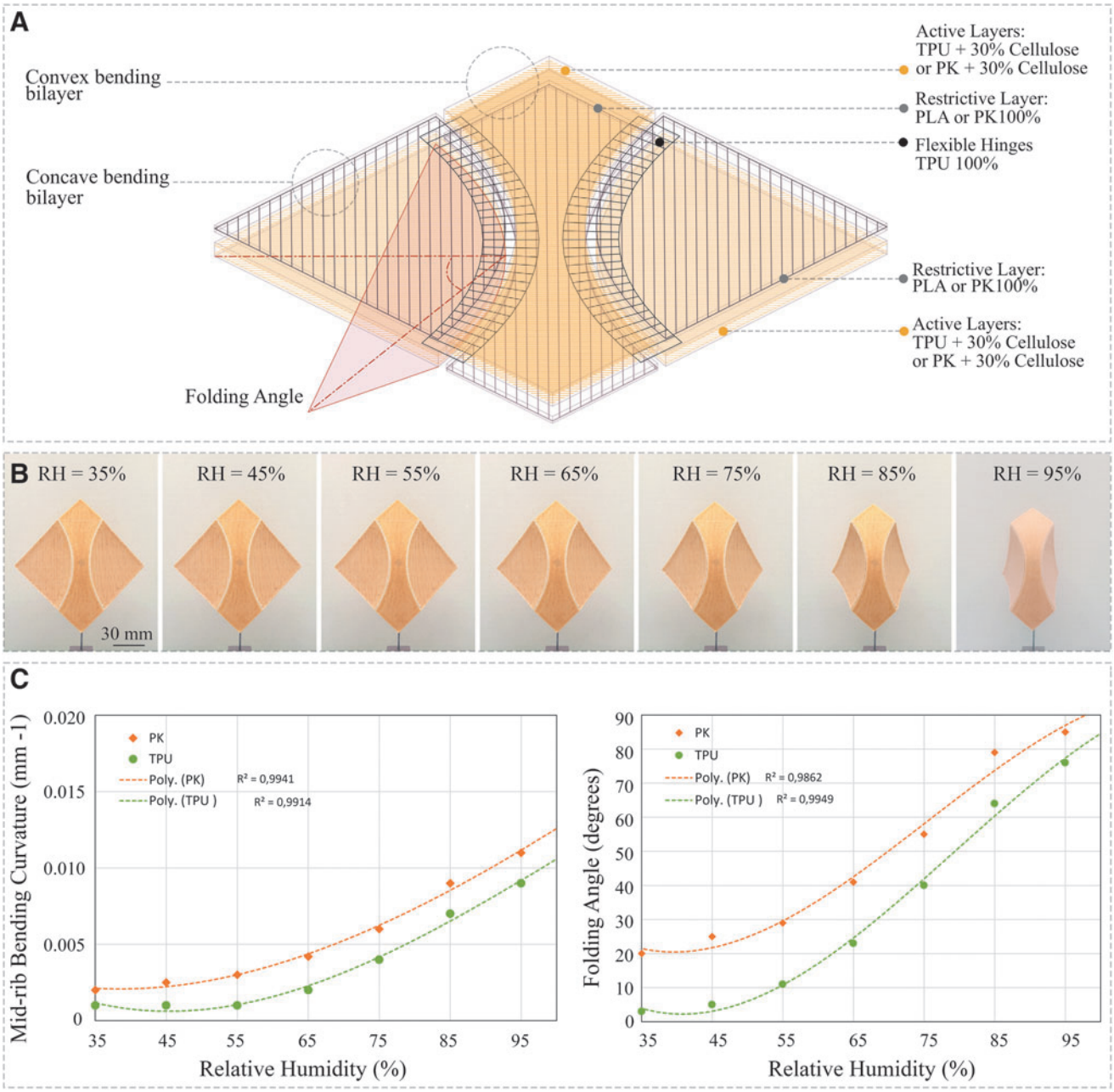

FIG. 6. Stepwise actuation of the bifold prototypes. **(A)** The mesostructure and toolpath design of the bifold module. **(B)** The curved folded prototype produced with PK-based filament as the active material, and its transformation from the flat to the folded state upon stepwise increase in the environment's RH. **(C)** Change of curvature in midrib face and the fold angle in the two prototypes (printed with PK70% and TPU70% filaments) through stepwise actuation (Supplementary Movie S2).

ranges, reaching on average 20% and 13% higher curvature in humid (RH = 95%) and wet states. This further confirms the effect of stiffness of the matrix polymer on the shape-change of the 4D-printed structures.[42,43]

Humidity-responsive smart structures

Functional bilayers can be aggregated to create composite structures with designed kinematics and adaptive functionalities. Following, we demonstrate two smart structures, as prototypes of adaptive shading elements in architectural building skins, that are designed to perform cyclic opening and closing in response to the environment's RH changes.

The first structure is an aperture module covered by five triangular bilayer flap elements. Each flap element, with approximate dimensions of $150 \times 100 \times 0.8$ mm, bends outward with a bending orientation perpendicular to the triangle fixed edge to open the aperture. The cyclic opening and closing of the aperture prototype, produced with the PK-based filament, is shown in Figure 4. At 35% RH level, all flaps are nearly flat, and the aperture is closed. A rise of RH to 90% RH results in the opening of the aperture, and a consecutive cycle of low RH results in the closing of the aperture (Fig. 4A). Moreover, this adaptation is fast.

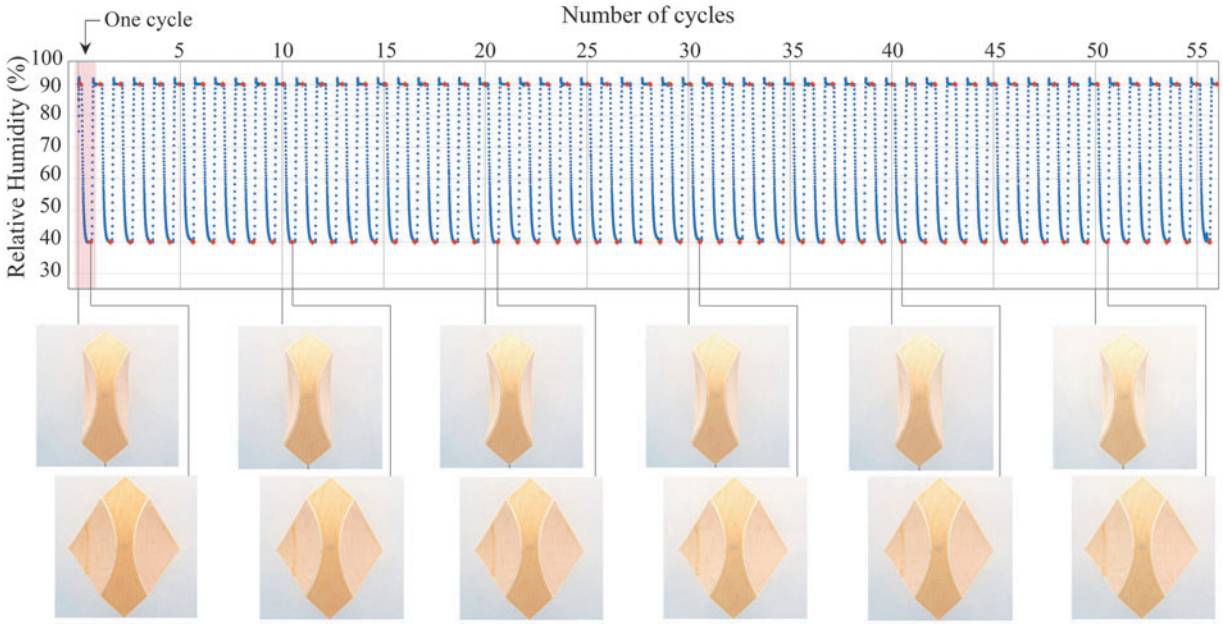

FIG. 7. Cyclic actuation of the bifold prototype. Time-lapse images of the bifold prototype, produced with PK70% filament, during 56 cyclic motions in response to alternating RH levels between 40% and 90% and a constant temperature of 20°C ± 1. The time in which each photograph is taken is marked with the *red marker* on the RH graph (Supplementary Movie S3).

In the absorption cycle, the aperture opens within ~35 min, which follows the changes of the RH level in the test chamber in real time (Fig. 4C). In the desorption cycles, the rate of closing is capped by the speed by which the test chamber lowers the RH level. An experiment was performed to measure the rate of shape-change upon immediate placement in preset 90% RH and 35% RH environments (Fig. 5). In the desorption cycle in 35% RH (from initial equalization in 90% RH), the aperture undergoes its major closing within the first 25 min, reaching more than 90% of its final shape-change. The equalization is reached within 75 min (Fig. 5A). Similarly, in the absorption cycle in 90% RH (from initial equalization in 35% RH), the prototype undergoes its major shape-change within the first 25 min, and it equalizes with the environment in 65 min (Fig. 5B).

In addition, the rate of shape-change through water immersion was measured. As shown in Figure 5C, the prototype reaches more than 90% of its shape-change within 14 min, and it reaches its final curvature in 34 min.

The second structure utilizes a self-shaping curved folding mechanism[35] to amplify the shape-change by translating smooth bending into folding with sharp angles (Fig. 6). In this study, the folding is achieved through distributed actuation of the bilayer faces, which are connected through flexible hinges along the curved creases. Upon bending of the adjacent bilayers in opposite convex and concave directions, the hinges flex, which results in the folding of the overall structure. Thus, a key requirement for the 4D printing of curved-folded mechanisms is the combination of compatible stiff and flexible, and active and restrictive materials in multilayered structures. This has been achieved through using both TPU-based and PK-based filaments in multimaterial structures. Figure 6A demonstrates the design and the mesostructural setup of the ''bifold'' curved folded module (dimensions of $100 \times 10 \times 0.8$ mm).

In the two lateral faces, the bilayers are arranged to bend in a convex direction, and the printing paths are oriented transversally to achieve a bending orientation parallel to the curved creases. The midrib face bends in the opposite concave direction with a similar bending orientation. The faces are connected through flexible strands, printed with the TPU100% filament, which are spaced 2 mm to reduce the bending stiffness of the hinge zones and facilitate the folding of the structure (Fig. 6A).

Using the TPU70% and PK70% filament as the active material, two prototypes were printed and tested through stepwise actuation. Figure 6C shows the measurements of the bending curvature in the midrib face and the folding angle. As expected, an increase in the RH level results in increasing the curvature of all faces and a consequent folding of the overall module. In both prototypes, the main folding happens within the RH range of 55–95%. Compared with the stand-alone bilayers, the midrib face in both prototypes reaches a lower curvature, which is due to the mechanical constraints of the overall structure. Nevertheless, such bending curvature causes a large transformation in the form of folding in the overall structure, reaching an ~90° fold angle at 95% RH.

A further comparison can be made between the PK-based and the TPU-based prototypes. It is observable that, as opposed to the stand-alone bilayers, the PK-based bifold module reaches a higher folding angle compared with the TPU-based prototype. This can be explained by the mechanics of the curved folding, which requires high stiffness in the faces compared with the low stiffness on the hinges.

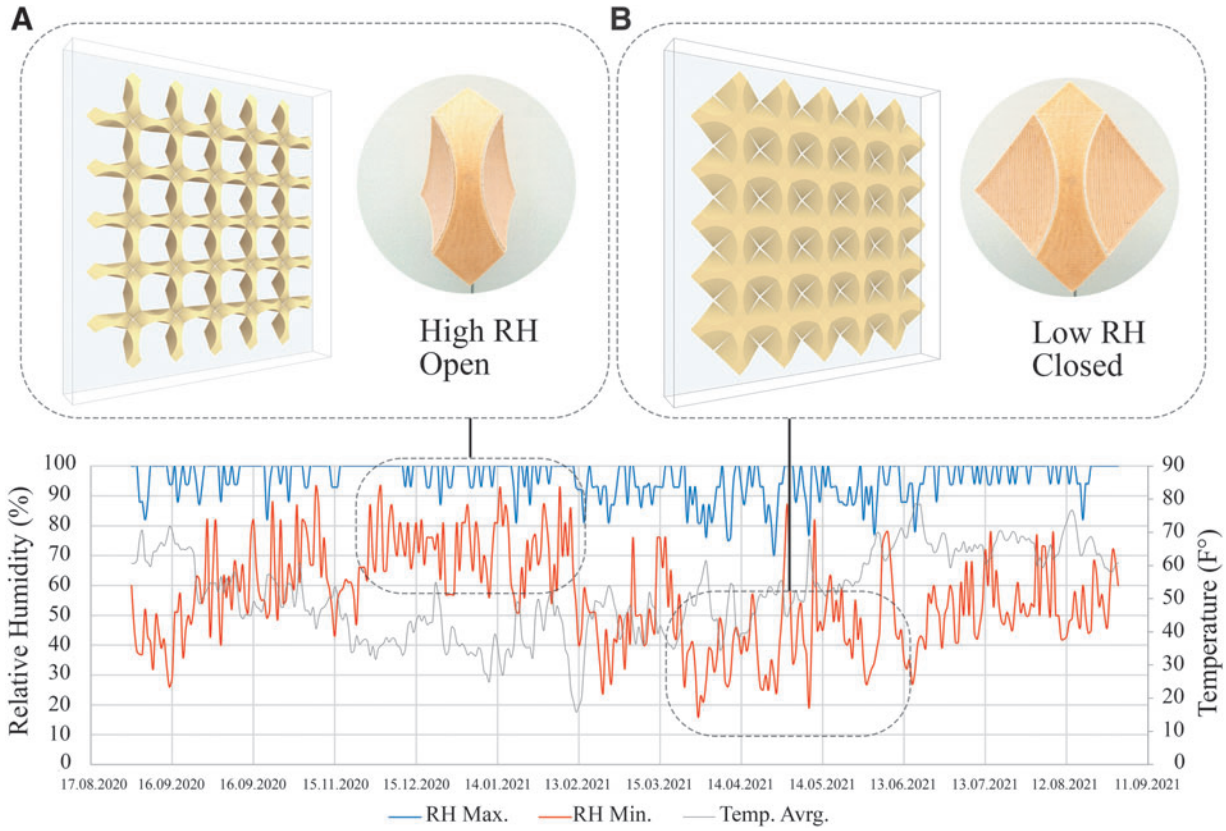

FIG. 8. Proposed application of the 4D-printed smart structures in weather-adaptive architectural building skins. **(A)** Open in high RH conditions (usually during fall/winter or at nights), **(B)** Closed to provide shading in low RH conditions (usually in hot and sunny summer time). The graph shows the minimum RH, maximum RH, and the average temperature from the EuroAirport Basel-Mulhouse-Freiburg weather station from September 1, 2020, to August 31, 2021.

Evaluation of long-term cyclic actuation

Last, we assessed the long-term, cyclic shape-change of the 4D-printed material system. For this purpose, the PK-based bifold prototype was actuated in alternating high (90%) and low (40%) RH in 3-h cycles for 14 days, resulting in 56 cycles of opening and closing (Fig. 7). The opening and closing of the prototype showed to be fully reversible and repeatable throughout the experiment. The prototype was able to reach a similar opening and closing area (±1%) in the last cycles compared with the first ones (Supplementary Fig. S5), showing no reduction in magnitude or speed of actuation. Furthermore, no mechanical damage (such as layer delamination or tearing) was visible in the prototypes, which confirms the durability of the 4D-printed material system in cyclic actuation.

Discussion

Through codesign, a pallet of biocomposite filament materials was specifically developed for 4D printing humidity-responsive structures. The use of pure cellulose powder as the hygroscopic filler, as opposed to wood flour typically used in commercial filaments, as well as using ductile matrix polymers resulted in enhanced responsiveness and shape-change in 4D-printed structures. This has a striking contrast with the previously shown 4D-printed hygromorphs,[22,23,44] which were only responsive to water immersion and could not perform adaptive functionalities purely from changes in ambient RH. The use of biobased polymers and native cellulose powder is valuable in terms of sustainability and the use of natural and renewable material resources, which contributes to the feasibility and scalability of production.

Compared with long-fiber natural composite material systems,[30,41] our produced filaments are printable on generic FFF desktop 3D printers without requiring any hardware modification. Utilizing the FFF toolpath design to tailor the mesostructure in the bilayers and program shape-change in larger motion mechanisms emphasizes the advantage of 4D printing over other manufacturing methods such as layer lamination or casting.

We then demonstrated a series of 4D-printed composite structures, which served as prototypes of humidity-responsive smart structures. All prototypes were able to achieve fully reversible cyclic opening and closing in response to the environment's RH, which overcomes some of the major shortcomings in the state of the art.[33] In terms of their adaptation speed, not only does the

prototype response time match the speed at which RH changes (both in the test chamber and in naturally occurring weather conditions), it is also observed to be faster than the state of the art in 4D-printed hygromorphs.[33] In addition, the presented experiments do not consider the impact of radiant heat, which can further accelerate the shape-change.

Comparing the TPU-based and PK-based samples, while the TPU-based stand-alone bilayer samples exhibited larger bending curvature upon absorbing moisture, the stiffer PK-based filaments allowed for reaching larger folding angles in the curved folded structures. Thus, it can be concluded that the PK-based filaments are favorable in developing mechanisms where higher stiffness is required, while the soft and flexible TPU-based filaments are valuable for applications where high conformability is desired, for example, in adaptive wearables.

Future work in terms of material development can explore a wider range of matrix polymers for filament production, with a special focus on fully biobased polymers. The recyclability of the biocomposite materials, potentially through remelting and mechanical recycling, is a topic of future investigations. The initial experiments have shown no signs of thermal degradation during viscosity measurements,[42] which is promising for potential mechanical recycling but requires further in-depth investigations. Another area for further research can focus on modeling the bilayer structures using fine element analysis or analytical methods. Specifically, the modified Timoshenko model[5,38] can be utilized to explore other bilayer layups with different combinations of TPU based and PK based, which may lead to discovering bilayer arrangements with larger shape-change or faster response times.

A promising outlook of this research is the application of the developed smart structures in weather-adaptive building envelopes (Fig. 8). For this, future work needs to examine the structures in variable natural conditions. The effect of ultraviolet radiation and radiant heat on the actuation speed, bending curvature, and longevity of the element needs to be considered in both the design and material engineering. Lastly, a long-term durability test in outdoor environments is needed to verify the practical applicability of the presented smart structures in adaptive architectural building envelopes.

Conclusion

This article presented a codesign approach for developing 4D-printed humidity responsive structures by incorporating the parallel development of customized biocomposite filament materials and architected mesostructures. This resulted in adaptive structures that are 3D printable on standard FFF 3D printers using biobased materials, are highly responsive to RH, and can perform cyclic motion in long term. This overcomes some of the major shortcomings in the current state of the art, including lack of adequate responsiveness to ambient humidity and weak reversibility and repeatability of motion in cyclic actuation. By utilizing biobased materials and renewable resources for the 4D printing of functional, passively actuated smart structures, these results open up new opportunities for weather-adaptive building skins that operate autonomously in response to natural shifts in RH.

Authors' Contributions

Conceptualization: Y.T., T.C., S.L., C.B., D.W., and A.M. Methodology: Y.T., T.C., S.L., and D.W. Investigation: Y.T., T.C., and S.L. Visualization: Y.T. Supervision: D.W., J.B., C.B., and A.M. Writing—original draft: Y.T. and D.W. Writing—review and editing: Y.T., T.C., S.L., J.B., C.B., D.W., and A.M.

Acknowledgments

We thank JELU-WERK and AKRO-PLASTIC for their supply of raw materials and additional datasheets. We also thank Dr. Philipp Koeser for his insightful comments and fruitful discussions, and Ekin Sila Sahin, Nima Zahiri, and Hooman Salyani for their help with developmental tasks that contributed to this work.

Author Disclosure Statement

All authors declare that they have no competing interests.

Funding Information

This work was funded by the German Federal Ministry of Food and Agriculture (sponsorship label 22018116) within the framework program Renewable Resources (FNR). Additional support was provided by the Deutsche Forschungsgemeinschaft (DFG, German Research Foundation) under Germany's Excellence Strategy—EXC 2120/1-390831618.

Supplementary Material

Supplementary Figure S1
Supplementary Figure S2
Supplementary Figure S3
Supplementary Figure S4
Supplementary Figure S5
Supplementary Movie S1
Supplementary Movie S2
Supplementary Movie S3

References

1. UN Environment Programme (UNEP). 2019 Global status report for buildings and construction sector. 2019. https://www.unep.org/resources/publication/2019-global-status-report-buildings-and-construction-sector (accessed November 29, 2021).
2. Menges A, Reichert S. Performative wood: physically programmiang the responsive architecture of the HygroScope and HygroSkin projects. Archit Des 2015;85:66–73.
3. Reichert S, Menges A, Correa D. Meteorosensitive architecture: biomimetic building skins based on materially embedded and hygroscopically enabled responsiveness. Comput Aided Des 2015;60:50–69.

4. Vailati C, Bachtiar E, Hass P, *et al.* An autonomous shading system based on coupled wood bilayer elements. Energy Build 2018;158:1013–1022.
5. Reyssat E, Mahadevan L. Hygromorphs: From pine cones to biomimetic bilayers. J R Soc Interface 2009;6: 951–957.
6. Holstov A, Farmer G, Bridgens B. Sustainable materialisation of responsive architecture. Sustainability 2017;9: 435.
7. Al-Obaidi KM, Azzam Ismail M, Hussein H, *et al.* Biomimetic building skins: an adaptive approach. Renew Sustain Energy Rev 2017;79:1472–1491.
8. Wood D, Vailati C, Menges A, *et al.* Hygroscopically actuated wood elements for weather responsive and self-forming building parts—facilitating upscaling and complex shape changes. Constr Build Mater 2018;165:782–791.
9. Wang W, Yao L, Cheng C-Y, *et al.* Harnessing the hygroscopic and biofluorescent behaviors of genetically tractable microbial cells to design biohybrid wearables. Sci Adv 2017;3:e1601984.
10. Zhong Y, Zhang F, Wang M, *et al.* Reversible humidity sensitive clothing for personal thermoregulation. Sci Rep 2017;7:44208.
11. Wei J, Jia S, Ma C, *et al.* Tough and multifunctional composite film actuators based on cellulose nanofibers toward smart wearables. ACS Appl Mater Interfaces 2021;13: 38700–38711.
12. Cheng T, Thielen M, Poppinga S, *et al.* Bio-inspired motion mechanisms: computational design and material programming of self-adjusting 4D-printed wearable systems. Adv Sci 2021;8:2100411.
13. Shin B, Ha J, Lee M, *et al.* Hygrobot: a self-locomotive ratcheted actuator powered by environmental humidity. Sci Robot 2018;3:eaar2629.
14. Lee Y, Song WJ, Sun J-Y. Hydrogel soft robotics. Mater Today Phys 2020;15:100258.
15. Kim K, Guo Y, Bae J, *et al.* 4D printing of hygroscopic liquid crystal elastomer actuators. Small 2021;17: e2100910.
16. Tibbits S. 4D printing: multi-material shape change. Archit Des 2014;84:116–121.
17. Momeni F, Mehdi Hassani NSM, Liu X, *et al.* A review of 4D printing. Mater Des 2017;122:42–79.
18. Kuang X, Roach DJ, Wu J, *et al.* Advances in 4D printing: materials and applications. Adv Funct Mater 2019;29: 1805290.
19. Zhang Z, Demir KG, Gu GX. Developments in 4D-printing: a review on current smart materials, technologies, and applications. Int J Smart Nano Mater 2019;10: 205–224.
20. Gladman AS, Matsumoto EA, Nuzzo RG, *et al.* Biomimetic 4D printing. Nat Mater 2016;15:413–418.
21. Correa D, Papadopoulou A, Guberan C, *et al.* 3D-printed wood: programming hygroscopic material transformations. 3D Print Addit Manuf 2015;2:106–116.
22. Correa D, Poppinga S, Mylo MD, *et al.* 4D pine scale: biomimetic 4D printed autonomous scale and flap structures capable of multi-phase movement. Philos Trans A Math Phys Eng Sci 2020;378:20190445.
23. Tahouni Y, Krüger F, Poppinga S, *et al.* Programming sequential motion steps in 4D-printed hygromorphs by architected mesostructure and differential hygro-responsiveness. Bioinspir Biomim 2021;16.
24. Mulakkal MC, Trask RS, Ting VP, *et al.* Responsive cellulose-hydrogel composite ink for 4D printing. Mater Des 2018;160:108–118.
25. Raviv D, Zhao W, McKnelly C, *et al.* Active printed materials for complex self-evolving deformations. Sci Rep 2014;4:7422.
26. Guo G, Wu Q, Liu F, *et al.* Solvent-cast-assisted printing of biomimetic morphing hydrogel structures with solvent evaporation-induced swelling mismatch. Adv Funct Mater 2021;32:2108548.
27. Cakmak O, El Tinay HO, Chen X, *et al.* Spore-based water-resistant water-responsive actuators with high power density. Adv Mater Technol 2019;4:1800596.
28. Le Duigou A, Castro M, Bevan R, *et al.* 3D printing of wood fibre biocomposites: from mechanical to actuation functionality. Mater Des 2016;96:106–114.
29. Krapež Tomec D, Straže A, Haider A, *et al.* Hygromorphic response dynamics of 3D-printed wood-PLA composite bilayer actuators. Polymers (Basel) 2021;13: 3209.
30. Le Duigou A, Barbé A, Guillou E, *et al.* 3D printing of continuous flax fibre reinforced biocomposites for structural applications. Mater Des 2019;180:107884.
31. Langhansl M, Dörrstein J, Hornberger P, *et al.* Fabrication of 3D-printed hygromorphs based on different cellulosic fillers. Funct Compos Mater 2021;2:4.
32. Milosevic M, Stoof D, Pickering K. Characterizing the mechanical properties of fused deposition modelling natural fiber recycled polypropylene composites. J Compos Sci 2017;1:7.
33. Le Duigou A, Correa D, Ueda M, *et al.* A review of 3D and 4D printing of natural fibre biocomposites. Mater Des 2020;194:108911.
34. Gauss C, Pickering KL, Muthe LP. The use of cellulose in bio-derived formulations for 3D/4D printing: a review. Compos Part C Open Access 2021;4:100113.
35. Tahouni Y, Cheng T, Wood D, *et al.* Self-shaping curved folding: a 4D-printing method for fabrication of self-folding curved crease structures. In: Symposium on Computational Fabrication (SCF '20). New York, NY, USA: Association for Computing Machinery, November 5, 2020; pp. 1–11.
36. Knippers J, Kropp C, Menges A, *et al.* Integrative computational design and construction: rethinking architecture digitally. Civil Eng Des 2021;3:123–135.
37. Cheng T, Tahouni Y, Wood D, *et al.* Multifunctional mesostructures: design and material programming for 4D-printing. In: Symposium on Computational Fabrication (SCF '20). New York, NY, USA: Association for Computing Machinery, November 5, 2020; pp. 1–10.
38. Krüger F, Thierer R, Tahouni Y, *et al.* Development of a material design space for 4D-printed bio-inspired hygroscopically actuated bilayer structures with unequal effective layer widths. Biomimetics 2021; 6:58.
39. Schindelin J, Arganda-Carreras I, Frise E, *et al.* Fiji: an open-source platform for biological-image analysis. Nat Methods 2012;9:676–682.

40. Mason D. Calculating properties of a triangle's circumcircle. Centre for Cell Imaging, 2017. https://bitbucket.org/davemason/threepointcircumcircle/src/master (accessed July 12, 2021).
41. Le Duigou A, Fruleux T, Matsuzaki R, *et al.* 4D printing of continuous flax-fibre based shape-changing hygromorph biocomposites: towards sustainable metamaterials. Mater Des 2021;211:110158,
42. Kliem S, Tahouni Y, Cheng T, *et al.* Biobased smart materials for processing via fused layer modeling. AIP Conf Proc 2020;2289:020034.
43. Fruleux T, Castro M, Sauleau P, *et al.* Matrix stiffness: a key parameter to control hydro-elasticity and morphing of 3D printed biocomposite. Compos Part A Appl Sci Manuf 2022;156:106882,
44. Vazquez E, Gürsoy B, Duarte JP. Formalizing shape-change: three-dimensional printed shapes and hygroscopic material transformations. Int J Archit Comput 2020;18: 67–83.

Address correspondence to:
Yasaman Tahouni
Institute for Computational Design and Construction (ICD)
University of Stuttgart
Keplerstrasse 11, 70174
Stuttgart
Germany

E-mail: yasaman.tahouni@icd.uni-stuttgart.de